

unperturbed correspondence and the rejuvenation occurred during t_2 . These 'memory effect' and 'rejuvenation' are observed in other experiments.³⁾

From the theoretical point of view, the aging phenomena have been studied along two different pictures. One is the droplet picture,^{10,11)} where the behavior in the spin glass phase is governed by the low laying and large length scale excitation. The other is the so-called hierarchical picture,^{12,13,14,15,16)} from which we will try to understand the phenomena in this manuscript.

According to the Parisi mean-field solution of the SK model, the free energy in the spin-glass phase has a very complex structure with numerous local minima. These valleys are considered to be divided into smaller valleys as the system is cooled and micro phase transitions occur with this continuous multifurcation. From this hierarchical structure, the memory effect and rejuvenation mentioned above can be explained as follows.⁸⁾ When the temperature is cooled from temperature above T_c down to T , the system falls into one of the numerous local minima. Then, the system is equilibrated in some region of the phase space including several valleys, \mathcal{R} , during t_1 . Now we consider to change the temperature from T to $T \pm \Delta T$. In the case $-\Delta T$, each valley at T is divided into smaller valleys. If ΔT is large enough and the time t_2 is not so long, the equilibration proceeds only in the smaller valleys and we can ignore the possibility that the system overcomes the barrier which separates the bigger valleys at T . Therefore, when the temperature is raised back to T and smaller valleys merge, we find that the system are unchanged during t_2 and the memory effect appears. In the case $+\Delta T$, on the other hand, several valleys in \mathcal{R} merge into one valley and the system forges the equilibration at T . Thus the system is rejuvenated.

This explanation is, however, quite qualitative and there exists no theoretical model which reproduces these features along this hierarchical picture. In this manuscript, we study the Multi-layer Random Energy Model (MREM)^{16,17,18)} which has a hierarchical structure causing a continuous phase transition. We introduce magnetization to this model so that we can carry out the simulation to observe the ac-susceptibility, and find that the memory effect and rejuvenation are indeed reproducible. Furthermore, we analyze the mechanism of these phenomena and show that the above-mentioned scenario realizes these features, at least, in this model.

Another feature we are interested in is the *chaos* effect found in experiments on the ac-susceptibility.¹⁹⁾ The fact found is that the equilibration at the temperature T does not affect the relaxation at a lower temperature $T - \Delta T$. This can be interpreted as follows. If the structure of the free energy at $T - \Delta T$ is quite different from that at T , the equilibration at T never helps the equilibration at $T - \Delta T$. But this reorganization of structure makes us unable to explain the memory effect, which is also observed in the same experiment. There seem to exist few theoretical explanations for these apparently conflicting features, i.e., memory and *chaos* effects. We find that these conflicting features hold simultaneously in the MREM in a situation slightly different from the experiment in ref. 19. We also analyze the mechanism of these phenomena in this model.

§2. The Multi-layer Random Energy Model

Let us first explain the Simple-layer Random Energy Model (SREM) illustrated in Fig. 1. The bottom points represent the accessible states of this system. We hereafter consider the case that the number of states is very large. The length of each branch represents the barrier energy E , over which the system goes from one state to another. This energy is an independent random variable distributed as

$$\rho(E)dE = \frac{dE}{T_c} \exp[-E/T_c], \quad (2.1)$$

where T_c is the transition temperature.

From the Arrhenius law, the relaxation time $\tau(\alpha)$, i.e., the average time for the system to escape from the state α , is related to $E(\alpha)$ as

$$\tau(\alpha) = \tau_0 \exp[E(\alpha)/T],$$

where τ_0 is a microscopic time scale. From eq. (2.1), the distribution of τ can be written as

$$p(\tau)d\tau = \frac{x\tau_0^x}{\tau^{x+1}}d\tau \quad (\tau \geq \tau_0), \quad (2.2)$$

where $x \equiv T/T_c$. From eq. (2.2), it is easily shown that the averaged relaxation time $\langle \tau \rangle$ is $\tau_0 x/(x-1)$ for $x > 1$ and infinite for $x \leq 1$. This means that the transition from the ergodic phase to the non-ergodic phase occurs at T_c .

Now we construct the Multi-layer Random Energy Model (MREM). As shown in Fig. 2, this model is constituted by piling up the SREM L times hierarchically. The energy of the n -th layer counted from the bottom, E_n , is given according to the distribution $\rho_n(E_n) = \exp[-E_n/T_c(n)]/T_c(n)$ and each layer has a different transition temperature chosen so as to satisfy $T_c(1) < T_c(2) < \dots < T_c(L)$. Therefore, in this model the transition occurs continuously from the uppermost (the L -th) layer to the lowest one.

2.1 The dynamics

In this simulation, we use the following Markoff process for dynamics. First the system is thermally activated from α to α_1 , where α_n is the n -th *ancestor* of α (see Fig. 2). The probability that this event occurs at time t in unit time is defined as

$$\omega(\alpha; t) = \tau_0^{-1} \exp[-E_1(\alpha)/T]. \quad (2.3)$$

The t dependence comes implicitly from time variation of temperature and magnetic field. We will introduce the effect of magnetic field in the following subsection. Since the time evolution is Markoffian, we can easily evaluate the probability $q(\alpha; t_0, t)dt$ for the event to occur during t and $t + dt$ with knowing that the system is in the state α at time t_0 as

$$q(\alpha; t_0, t)dt = \omega(\alpha; t)dt \exp[-\int_{t_0}^t dt' \omega(\alpha; t')]. \quad (2.4)$$

We generate an event time t according to $q(\alpha; t_0, t)$ to perform event-driven Monte Carlo simulation.

Once the event occurs and the system is activated to α_1 , it may be activated further to α_2 , α_3 or higher branching point. We accept the excitation to α_2 with the probability $\exp[-E_2(\alpha)/T]$. If it is accepted, the next trial to α_3 follows. By repeating these procedures, we obtain the probability $H(n)$ that the system is activated from α_1 up to α_n as

$$H(n) = (1 - \exp[-E_{n+1}(\alpha)/T]) \prod_{k=2}^n \exp[-E_k(\alpha)/T], \quad (2.5)$$

where $E_{L+1}(\alpha) \equiv \infty$.

Finally, we adopt the simplest falling process from α_n . The system falls to one of all states under α_n with equal probability. In the limit that the number of branches in each layer is infinite, we can neglect the possibility that the system has visited one state more than twice in our finite time simulation. Therefore, in this simulation, we create a new state β after each activation. Note that if the system is activated to n -th layer, we set $E_k(\beta) = E_k(\alpha)$ for $k \geq n + 1$, although for $k \leq n$, E_k is updated according to the density of state $\rho_k(E)$.

We note that the whole process drives the system to the equilibrium distribution proportional to $\exp[\sum_n E_n/T]$.

2.2 Assignment of magnetization

In order to observe the magnetic response, we introduce magnetization to the MREM. It is natural to suppose that the nearer two states are located in the phase space the stronger the correlation of the two magnetizations is, and that the distance in the MREM can be measured in terms of barrier height. In fact the barrier height is related with the overlap in the SK model.²⁰⁾ To incorporate this aspect, we assign the value of magnetization to state α , M_α , as

$$M_\alpha = \mathcal{M}_0(\alpha) + \mathcal{M}_1(\alpha_1) + \cdots + \mathcal{M}_{L-1}(\alpha_{L-1}), \quad (2.6)$$

where $\mathcal{M}_k(\alpha_k)$ is a contribution from the branch point α_k given as a independent random variable with zero mean. The correlation between M_α and M_β with the lowest common branch point α_k comes from the common contributions of \mathcal{M}_n , ($n = k, k+1, \cdots$) to these magnetization. It decreases monotonically as k increases and the barrier becomes higher.

In this simulation, we choose a uniform distribution for \mathcal{M} of the n -th layer as

$$D_n(\mathcal{M}) = \begin{cases} \frac{\sqrt{L}}{2} & (|\mathcal{M}| \leq \frac{1}{\sqrt{L}}), \\ 0 & (|\mathcal{M}| > \frac{1}{\sqrt{L}}). \end{cases} \quad (2.7)$$

The range of distribution is determined so that the variance of M_α is independent of L .

The Zeeman energy due to applying magnetic field $H(t)$ is attributed to the lowest layer and $E_1(\alpha)$ in eq. (2.3) is replaced with $E_1(\alpha) + H(t)M_\alpha$.

To summarize, we introduce the concrete procedure of our simulation.

- (i) Choose the initial state α . Because we consider the situation that the system is quenched from infinitely high temperature, we determine $E_k(\alpha)$ ($k = 1, \dots, L$) according to $\rho_k(E)$. We also determine $\mathcal{M}_k(\alpha)$ from $D_k(\mathcal{M})$.
- (ii) Determine the time t_{stay} that the system stay at α from eq. (2.4).
- (iii) Determine how far the system is activated by eq. (2.5).
- (iv) Give the energy and magnetization of new state β . When the system is activated to α_n , we set $E_k(\beta) = E_k(\alpha)$ and $\mathcal{M}(\beta) = \mathcal{M}(\alpha)$ for $k \geq n + 1$ and give $E_k(\beta)$ and $\mathcal{M}(\beta)$ from $\rho_k(E)$ and $D(\mathcal{M})$ for $k \leq n$.
- (v) Set the time ahead by t_{stay} and return to (ii).

We show an example of simulation for $L = 2$ with a weak ac-field. We plot $\mathcal{M}_k(t)$ ($k = 1, 2$) in one trial in Fig.3(a), and averaged magnetization over 2×10^7 trials in Fig.3(b). We can see that in one trial, \mathcal{M}_k keeps a constant during the system stays at a state and changes discontinuously when activation occurs. We can see that the activation to the 1-st layer and the one to the 2-nd layer occurs at t_2 and t_1 respectively. From this figure, we can not find the effect of ac-field. But this effect emerges by taking average over numerous trials, as shown in Fig. 3(b). We estimate $\chi''(t)$ directly from data of this kind.

§3. The Result of Simulations

In the following we show the result of simulations performed on the MREM with $L = 2$, $T_c(1) = 0.6$ and $T_c(2) = 1.0$. The number of samples used for random average is typically 10^7 . The amplitude and the period of applying ac-field are fixed to 0.1 and $100\tau_0$, respectively. Hereafter this period is used as the unit of time.

3.1 The case $-\Delta T$

In the first stage the system evolves in temperature $T = 0.85$ for time interval t_1 . Temperature is then reduced to $T - \Delta T = 0.5$ for t_2 (the second stage), and brought back to T in the following third stage. Note that these temperatures are set so as to satisfy

$$T - \Delta T < T_c(1) < T < T_c(2).$$

In Fig. 4, we plot imaginary part of ac-susceptibility, χ'' , for two different intervals of the first stage, $t_1 = 20$ and 100. In inset we plot t_1 and t_3 part of data. We can see that the memory effect takes place. We also find in the data for $t_1 = 100$ the slight jump at the beginning of the second stage as seen in experiment.⁷⁾

In Fig. 5, we plot χ''_0 and χ''_1 evaluated from \mathcal{M}_0 and \mathcal{M}_1 , respectively ($\chi'' = \chi''_0 + \chi''_1$). We can see that χ''_0 remains almost constant in the first and third stage because $T > T_c(1)$ so that the first layer quickly relaxes to the equilibrium. The long-time dependence of relaxation is dominated by the second layer there. In contrast the first layer is dominant in the second stage because $T - \Delta T$

is too low for the second layer to be activated and χ_1'' is much smaller than χ_0'' . From these results, we notice that the dominant layer changes as temperature varies.

we can also see that the slight jump of χ'' mentioned above is brought from χ_0'' . This sudden increase of χ_0'' is due to the quenching of the first layer across its transition temperature $T_c(1)$.

In Fig. 6, χ_s'' in the second stage is magnified for $t_1 = 20$ and $t_1 = 100$. There are few differences on both χ_0'' and χ_1'' . This means that the length of the first stage, t_1 , does not affect the relaxation in the second stage. In this sense, we may say that the system has the *chaos* effect. On the other hand, t_1 reflects on relaxation in the third stage and the memory effect appears. Thus the MREM has these two apparently conflicting features simultaneously.

In order to investigate which states contribute to χ'' in more detail, we examine the energy distribution $P_n(E_n, t)$ which is defined as the probability density that the system is found at time t in one of the states whose energy of the n -th layer is E_n . By the definition, we have $P_n(E_n, t = 0) = \rho_n(E_n)$ since the initial state is chosen randomly.

In Fig. 7, we show the time dependence of $P_n(E_n, t)$ in the first stage. We can see that the distribution consists of two exponential functions which are connected to each other at some point, E^* . The value of E^* roughly represents the energy level up to which the system can be activated during time interval t , and is estimated as

$$E^* \approx T \log[t/\tau_0]. \quad (3.1)$$

For $E_n \leq E^*$ the distribution is aged or equilibrated, so that the exponent $\alpha_1(n)$ is given as

$$\alpha_1(n) = \frac{1}{T} - \frac{1}{T_c(n)}, \quad (3.2)$$

while the other part $E_n \geq E^*$ leaves untouched and the exponent $\alpha_2(n)$ is equal to that of $\rho_n(E)$, i.e.,

$$\alpha_2(n) = -\frac{1}{T_c(n)}. \quad (3.3)$$

For the first layer we have $\alpha_1(1) < 0$ since $T > T_c(1)$, and the distribution quickly converges to the equilibrium one (Fig.7, left). Note that the discrepancy for $E_1 > E^*$ is negligible in magnitude. For the second layer where $\alpha_1(2) > 0$, on the other hand, $P_2(E_2, t)$ has a peak at E^* moving right with time (Fig. 7, right). This is why χ_1'' continues to change with time while χ_0'' remains almost constant in the first stage.

Experiments on the Zero-Field-Cooled (ZFC) magnetization in spin glasses^{1,2)} showed that the distribution of the relaxation time τ , which has a peak at τ_{\max} , depends on the waiting time t_w and τ_{\max} appears near t_w , which just corresponds to the shift of peak shown in the right of Fig. 7.

In Fig. 8, we show the time dependence of $P_n(E_n, t)$ in the second stage. We can see that a peak appears and moves to right for the first layer (Fig. 8, left). As for $P_2(E_2, t)$, the global aspects such as the position of peak formed in the first stage do not change although the distribution of the lower energy decreases gradually. This brings the memory effect to the system.

To see how t_1 affects the energy distribution, we plot in Fig. 9 $P_n(E_n, t)$ for $t_1 = 20$ and $t_1 = 10^2$ with the same t in the second stage. As for the first layer, the both distributions are almost the same since the layer is well equilibrated in the first stage. In the second stage, this layer is dominant and the behaviors of χ'' are almost the same in the two cases. On the other hand, the difference of the peak position quenched since the end of first stage, makes the shapes of $P_2(E_2, t)$ very different from each other, and this causes, in turn, the difference in the behavior of χ'' in the third stage.

3.2 The case $+\Delta T$

In Fig. 10, the χ'' for the case $+\Delta T$ is shown. The heating is done twice in this case. We set the temperatures as $T = 0.5$, $T + \Delta T = 0.85$, which satisfy the relation $T < T_c(1) < T + \Delta T < T_c(2)$. We can see from this figure that the rejuvenation occurs.

We show the behavior of χ_0'' and χ_1'' in Fig. 11. In this case we can see that the χ_1'' dominates the slow relaxation in the second and fourth stages as expected. The rejuvenation occurs only in χ_0'' but not in χ_1'' .

In Fig. 12, we compare the behavior of χ'' in the first, third and fifth stages. Although the value in the first stage is slightly larger than that in the third, those in the third and fifth stages are collapsed to a single curve, which means the perfect re-initialization.

We again examine $P_n(E_n, t)$ in this case. In Fig. 13, the time evolution of $P_1(E_1, t)$ in the second stage is shown. The peak created in the first stage is rapidly destroyed and the information on the relaxation in the first stage is completely forgotten. In fact we find that the peak starts to disappear at $t \simeq t_1 + 1$, i.e., just after the second stage begins.

§4. Conclusions and Discussions

We have shown that the present MREM can reproduce the prominent behaviors found in spin glasses such as the memory effect and the rejuvenation although the number of layers is only two. This indicates that the alternation of the activated layer is important to explain these features in this model. We expect that the phenomena can be observed at any $T < T_c$ in the MREM with large L .

Now let us discuss what happens when $L \gg 1$ along the scenario proposed by Bouchaud and Dean.¹⁶⁾ For a given temperature $T < T_c(L) = T_c$, there exists the n -th layer such that $T_c(n-1) < T < T_c(n)$. The essential point is the fact that layers below n are quickly equilibrated and they forget what happened before the temperature is set, while those above n are almost quenched and they behave as if the time evolution stops. In this sense the n -th layer is the *activated* one and dominates the relaxation of the system. This mechanism certainly explains the memory effect and the rejuvenation as shown in the present work. In this context, the *chaos* effect means that the layer which is to be activated when temperature decreases is not capable to remember the previous situation and it relaxes from *tabulae rasae*. Therefore it is not necessary to introduce a *chaotic*

reorganization of hierarchy for description of the phenomena.

Finally, let us compare the droplet model with the MREM and try to fuse these models. In the droplet model, system *ages* by growth of droplets. On the other hand, aging means the shift of the peak of $P(E)$ in the *frozen* layers (the layers which satisfy $T < T_c(n)$) in the MREM. In both model, aging means to seek more stable states with time and these processes make the system stiffer and the response to an external field weaker. This is the reason why the ac-susceptibility decreases monotonously with age. Moreover, as discussed Jonason *et al.*,¹⁹⁾ it may be possible to map the MREM into the droplet model as following. We now consider what will happen when we cool real spin glass systems across the T_c (which corresponds to $T_c(L)$ in the MREM). Above T_c , all the spins flip rather free. When the system is cooled just below T_c , we can consider that larger droplets are blocked at first and the spins in these droplets begin to flip collectively. In this stage, the spins in smaller droplet are still free relatively. In the MREM, the larger droplets correspond to the upper *frozen* layers and the smaller droplets correspond to the lower *unfrozen* layers. As the temperature is lowered, smaller droplets begin to be blocked and flip collectively. But the larger droplets which blocked earlier are almost frozen and they can hardly flip at this temperature. We expect that these successive processes bring the memory effect, rejuvenation and *chaos* effect as discussed in this manuscript. Furthermore, the idea of *droplets within droplets*²¹⁾ will naturally lead to the hierarchical organization of droplets. It is challenging to find these structures, if really exist, in the real spin space of spin glasses.

Acknowledgements

We are very grateful to H. Yoshino for fruitful discussions and suggestions on the manuscript. The numerical calculations were performed on an Origin 2000 at Division of Physics, Graduate school of Science, Hokkaido University.

-
- 1) P. Svedlindh, P. Granberg, P. Nordblad, L. Lundgren and H. S. Chen: Phys. Rev B **35**(1987)268.
 - 2) L. Lundgren, P. Svedlindh and O. Beckman: Phys. Rev B **26**(1982)3990.
 - 3) Ph. Refregier, E. Vincent, J. Hammann and M. Ocio: J. Phys. (Paris) **48**(1987)1533.
 - 4) P. Granberg, L. Sandlund, P. Nordblad, P. Svedlindh and L. Lundgren: Phys. Rev. B **38**(1988)7097.
 - 5) P. Granberg, L. Lundgren and P. Nordblad: J. Magn. Magn. Mater **92**(1990)228.
 - 6) J. O. Andersson, J. Mattsson and P. Svedlindh: Phys. Rev. B **46**(1992)8297.
 - 7) E. Vincent, J. P. Bouchaud, J. Hammann and F. Lefloch: Phil. Mag. B **71**(1995)489.
 - 8) F. Lefloch, J. Hammann, M. Ocio and E. Vincent: Europhys. Lett **18**(1992)647.
 - 9) J. O. Andersson, J. Mattsson and P. Nordblad: Phys. Rev. B **48**(1993)13977.
 - 10) D. S. Fisher and D. A. Huse: Phys. Rev. B **38**(1988)373.
 - 11) G. J. M. Koper and H. J. Hilhorst: J. Phys. (Paris) **49**(1988)429.
 - 12) M. Sasaki and K. Nemoto: J. Phys. Soc. Jpn **68**(1999)1148.
 - 13) H. Yoshino: J. Phys. A **30**(1997)1143.
 - 14) P. Sibani and K. H. Hoffmann: Phys. Rev. Lett **63**(1989)2853.

- 15) C. Schulze, K. H. Hoffmann and P. Sibani: Europhys. Lett **15**(1991)361.
- 16) J. P. Bouchaud and D. S. Dean: J. Phys. I France **5**(1995)265.
- 17) B. Derrida: J. Phys. Lett. France **46**(1985)401.
- 18) B. Derrida and E. Gardner: J. Phys. C **19**(1986)2253.
- 19) K. Jonason, E. Vincent, J. Hammann, J. P. Bouchaud and P. Nordblad: Phys. Rev. Lett. **81**(1998)3243.
- 20) K. Nemoto: J. Phys. A **21**(1988)L287.
- 21) J. Villain: J. Phys. France **46**(1985)1843.

FIGURE CAPTIONS

Fig. 1 Structure of the Simple-layer Random Energy Model.

Fig. 2 Structure of the Multi-layer Random Energy Model with $L = 2$.

Fig. 3 (a) $\mathcal{M}_1(t)$ (dashed line) and $\mathcal{M}_2(t)$ (solid line) observed in one trial and (b) averaged $\mathcal{M}_k(t)$ over 2×10^7 trials.

Fig. 4 χ'' for the case $-\Delta T$ with $t_1 = 20$ (dashed line) and $t_1 = 100$ (solid line). In the inset, the data in the first and third stage are plotted.

Fig. 5 χ_0'' (solid line) and χ_1'' (dashed line) for the case $-\Delta T$.

Fig. 6 χ'' in the second stage. χ_0'' with $t_1 = 20$, χ_0'' with $t_1 = 100$, χ_1'' with $t_1 = 20$ and χ_1'' with $t_1 = 100$ (from top to bottom).

Fig. 7 $P_n(E_n, t)$ in the first stage at $t = 1, 10^{0.5}, 10, \dots, 10^2$ (from left to right).

Fig. 8 $P_n(E_n, t)$ in the second stage at $t = 0, 10^{-1.5}, 10^{-1}, \dots, 10^2$ (from left to right).

Fig. 9 $P_n(E_n, t)$ for $t_1 = 20$ (left) and $t_1 = 100$ (right) in the second stage at $t = t_1 + 10^{1.5}$.

Fig. 10 χ'' for the case $+\Delta T$. In the inset, the tree parts of perturbed data and unperturbed data are shown.

Fig. 11 χ_0'' (upper) and χ_1'' (lower) for the case $+\Delta T$.

Fig. 12 χ'' in the first, third and fifth stages.

Fig. 13 $P_1(E_1, t)$ in the second stage for the case $+\Delta T$ at time $t = t_1 + \Delta t$ with $\Delta t = 10^{-1.5}, 10^{-1}, \dots, 10^2$.

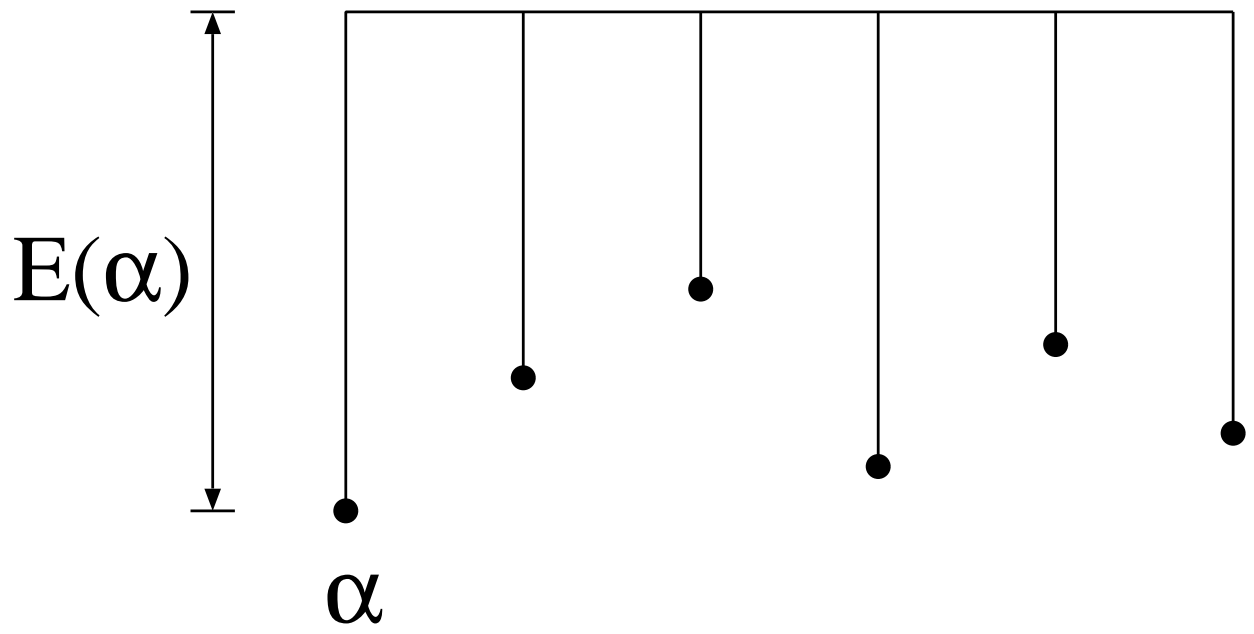


Fig.1

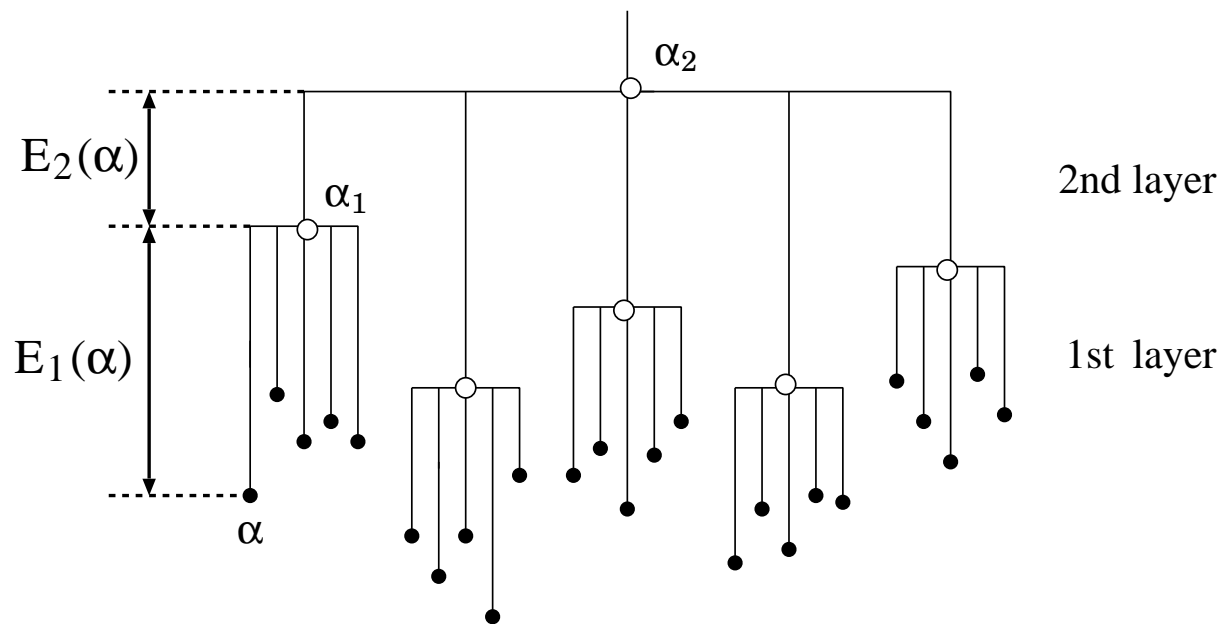


Fig.2

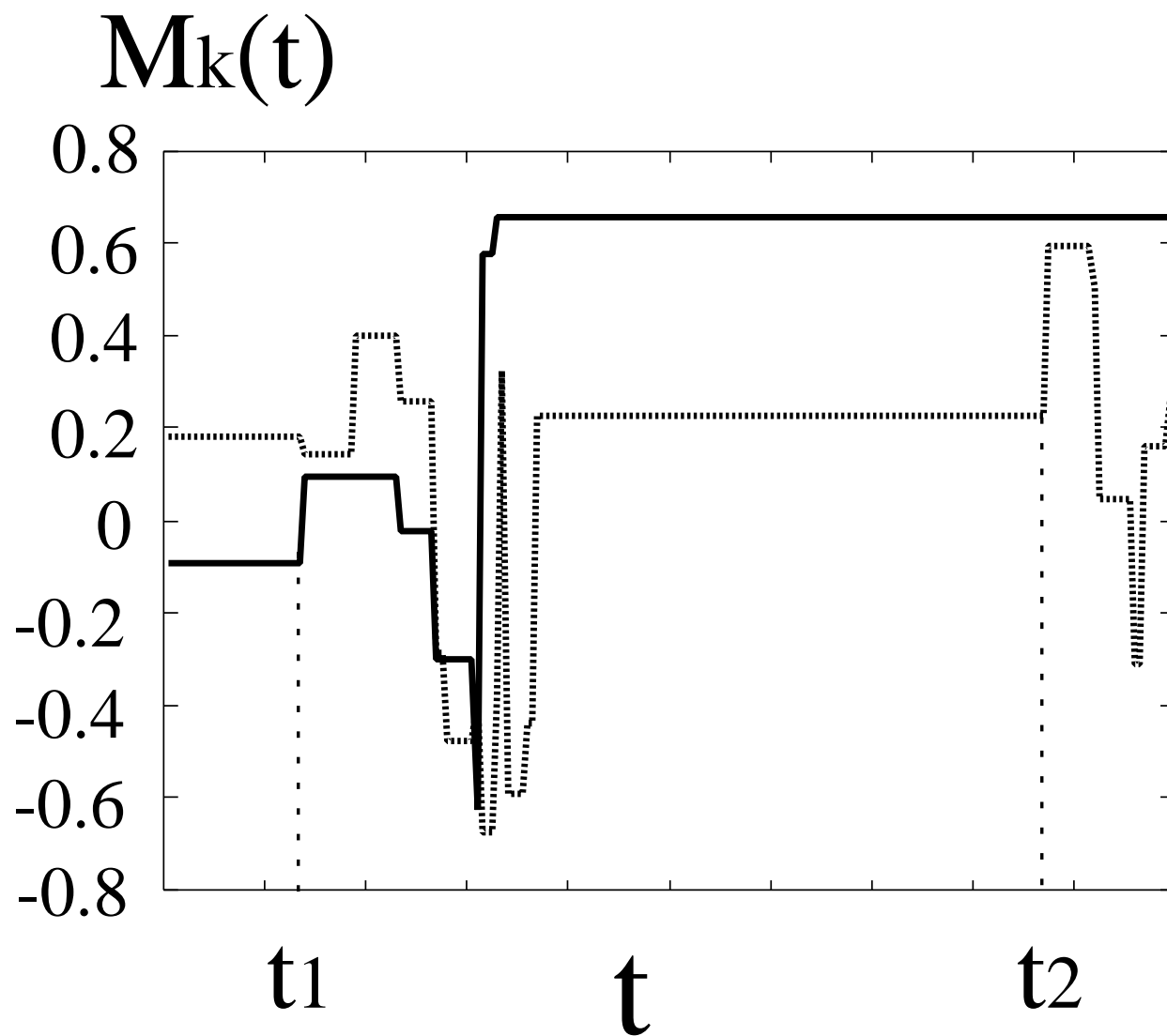


Fig.3(a)

$M_k(t)$

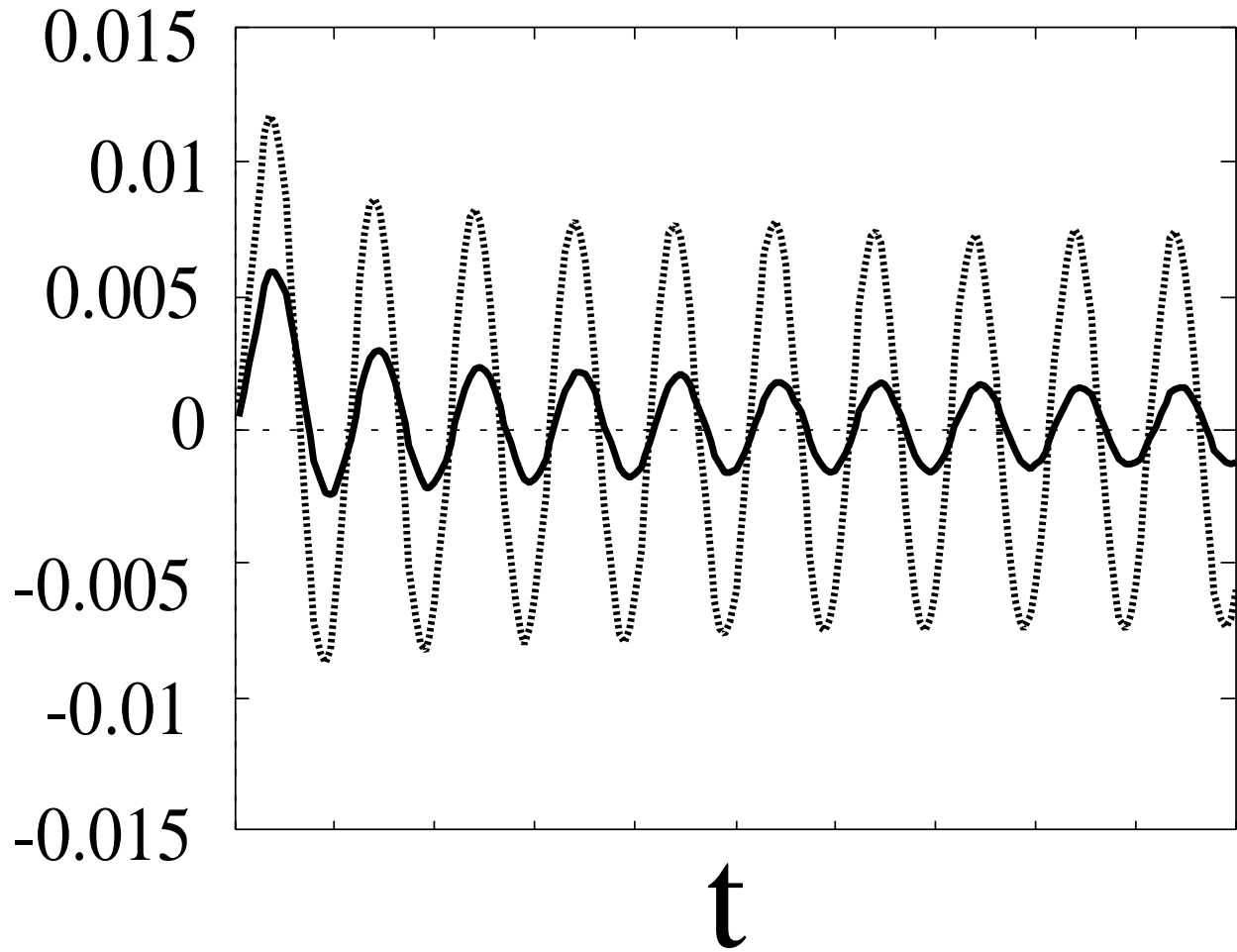


Fig.3(b)

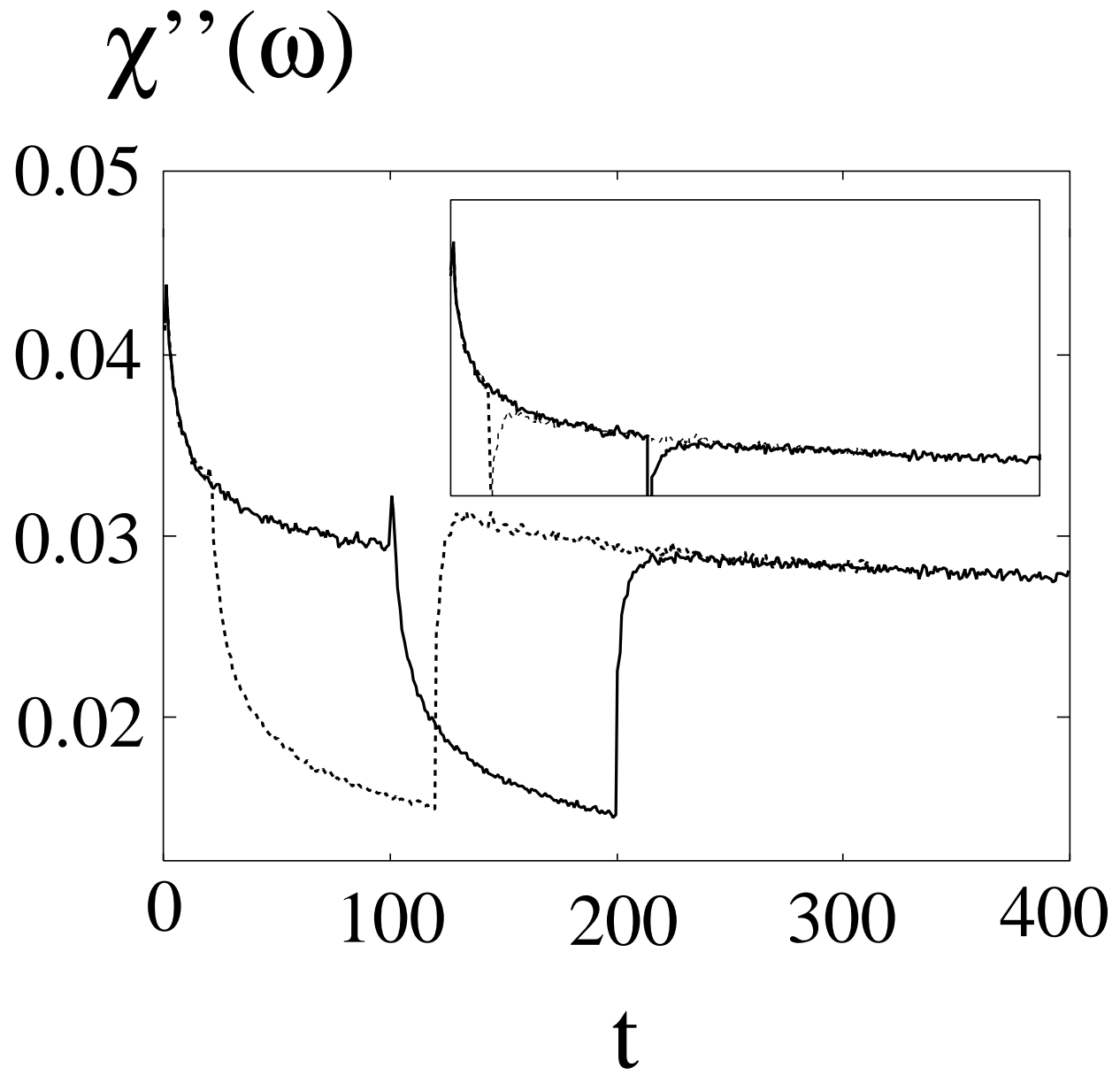


Fig.4

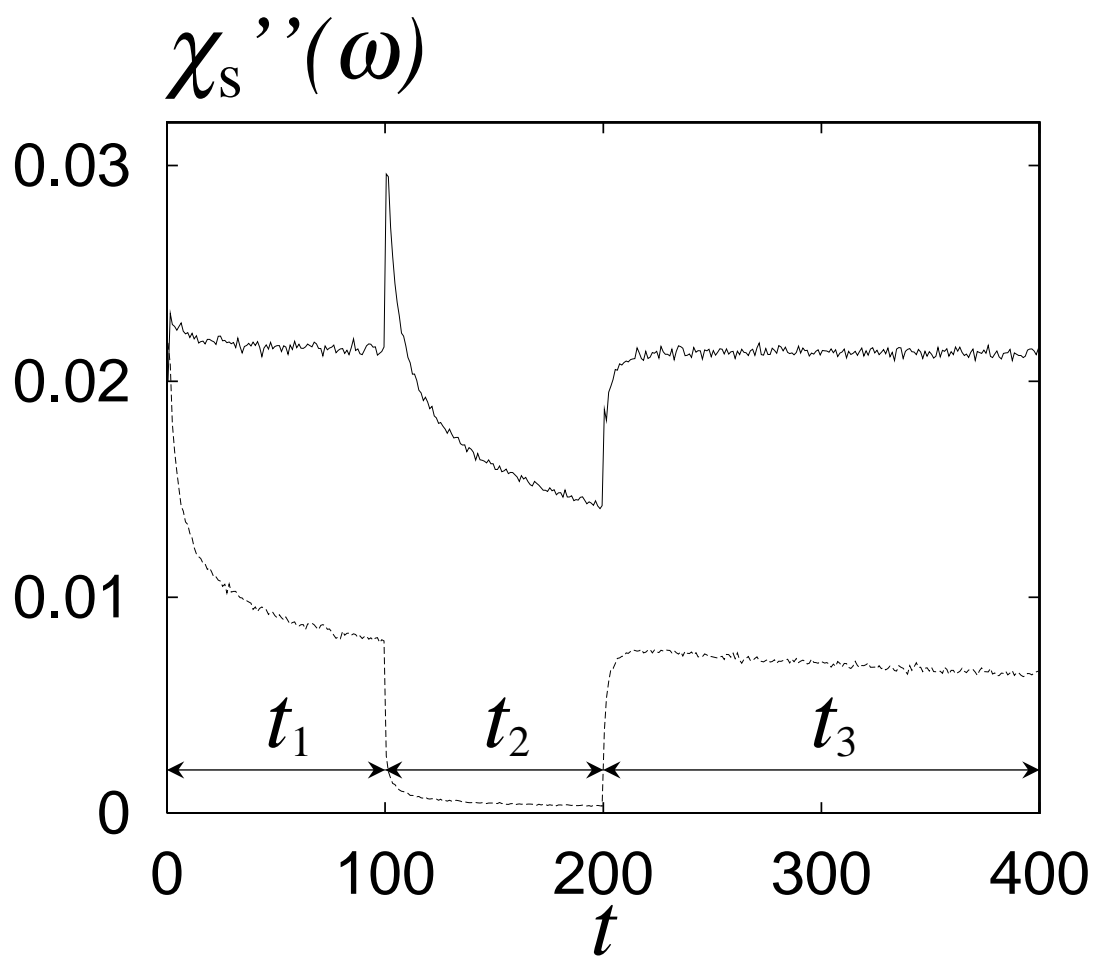


Fig.5

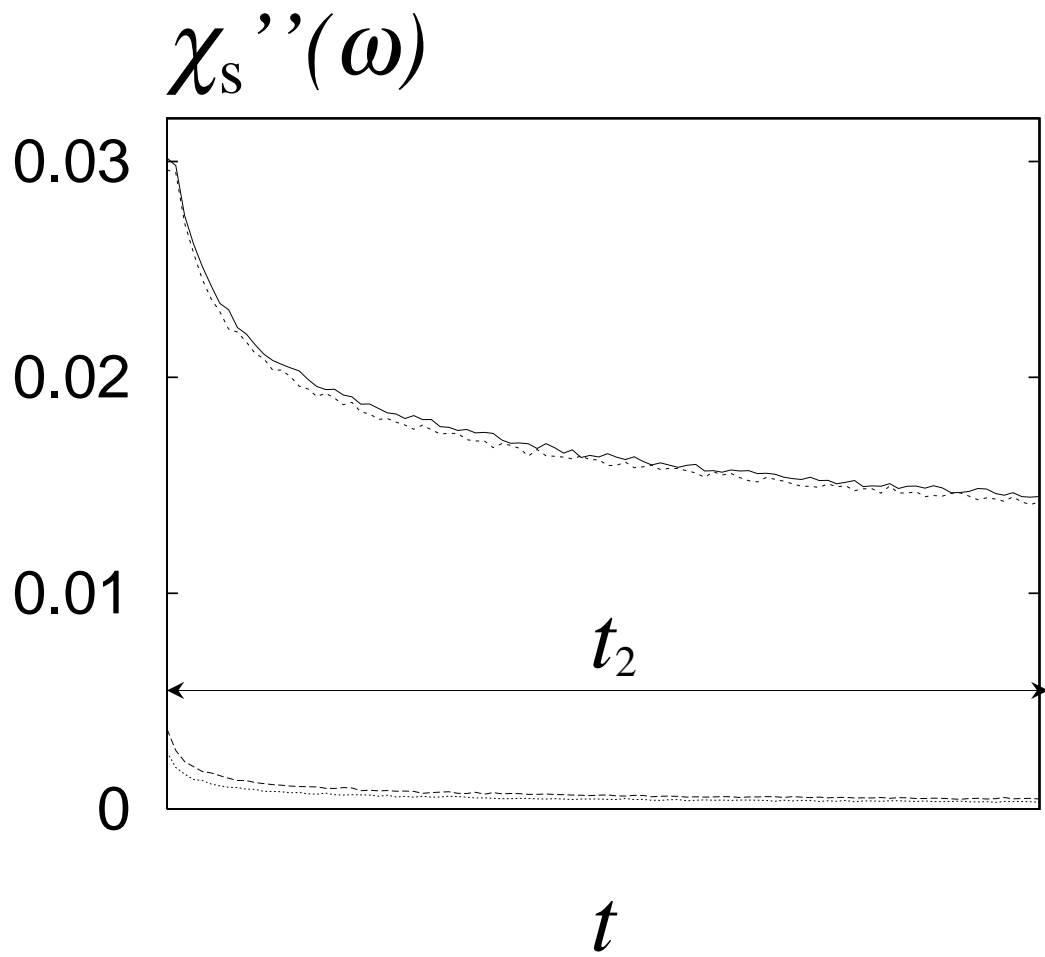


Fig.6

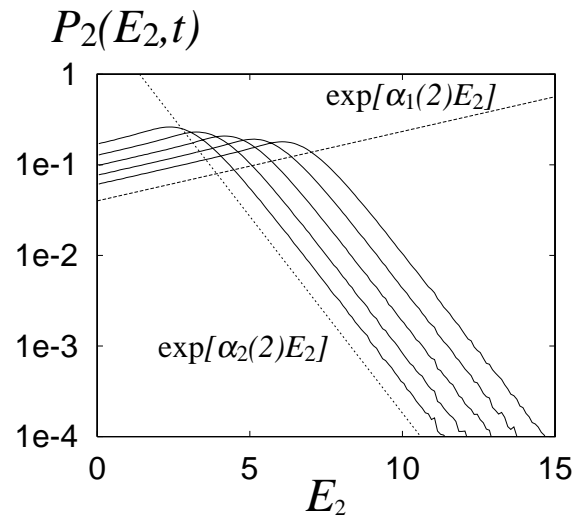
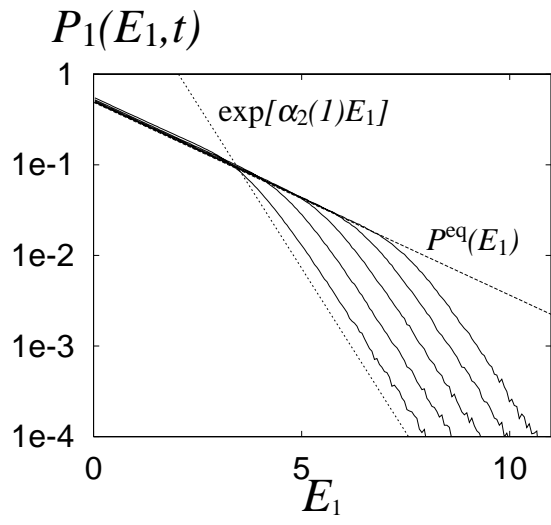


Fig.7

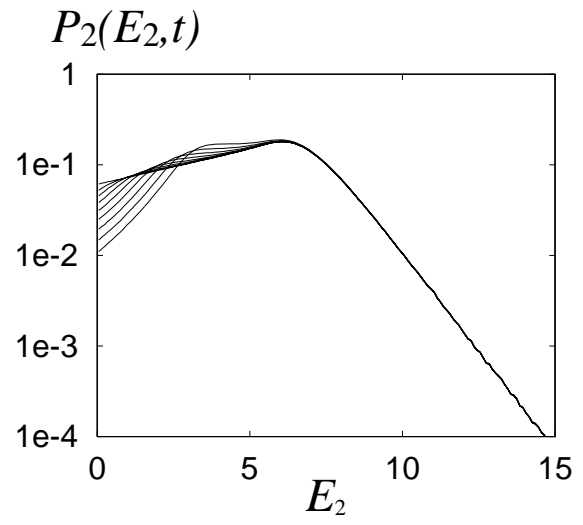
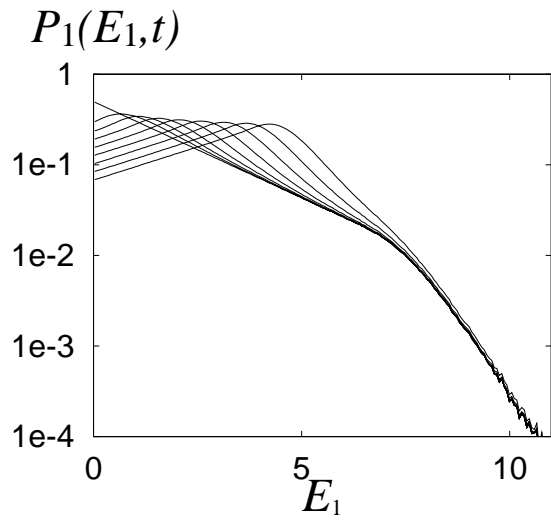


Fig.8

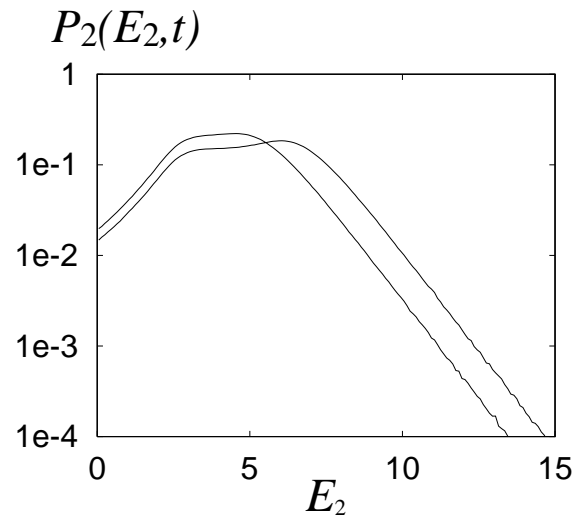
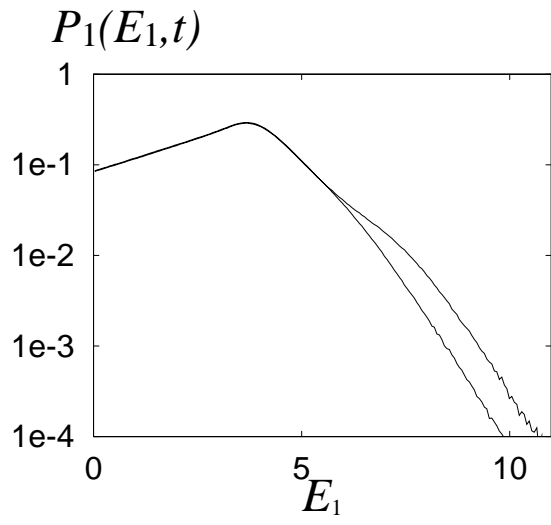


Fig.9

$$\chi''(\omega)$$

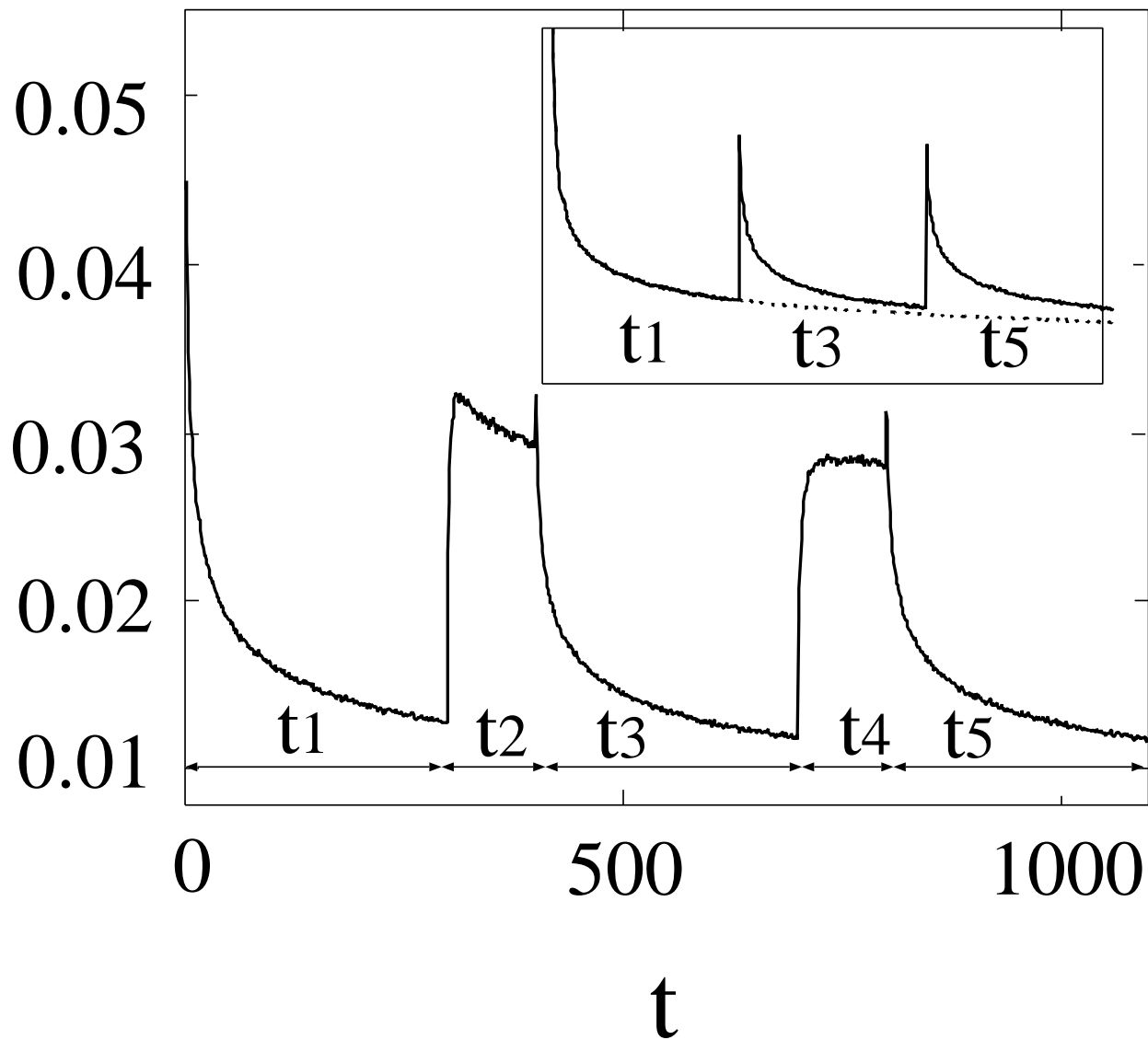


Fig.10

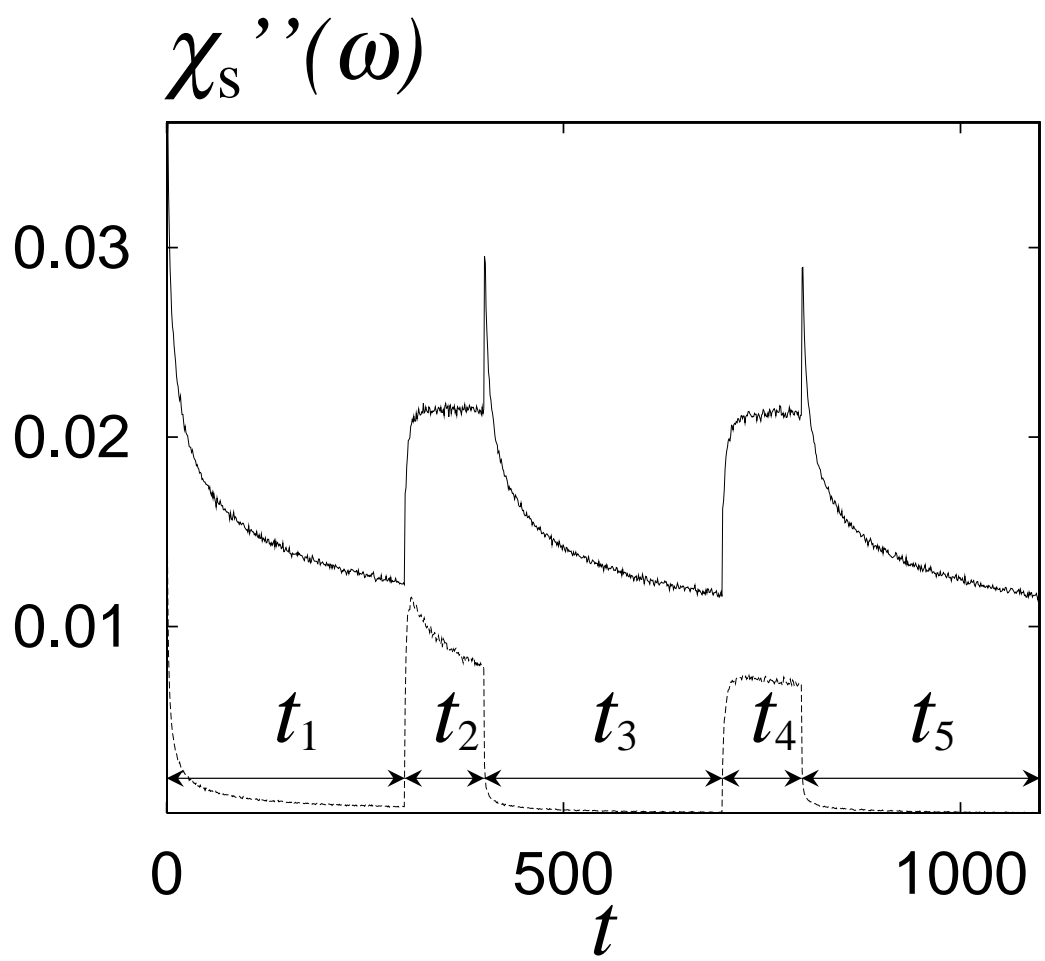


Fig.11

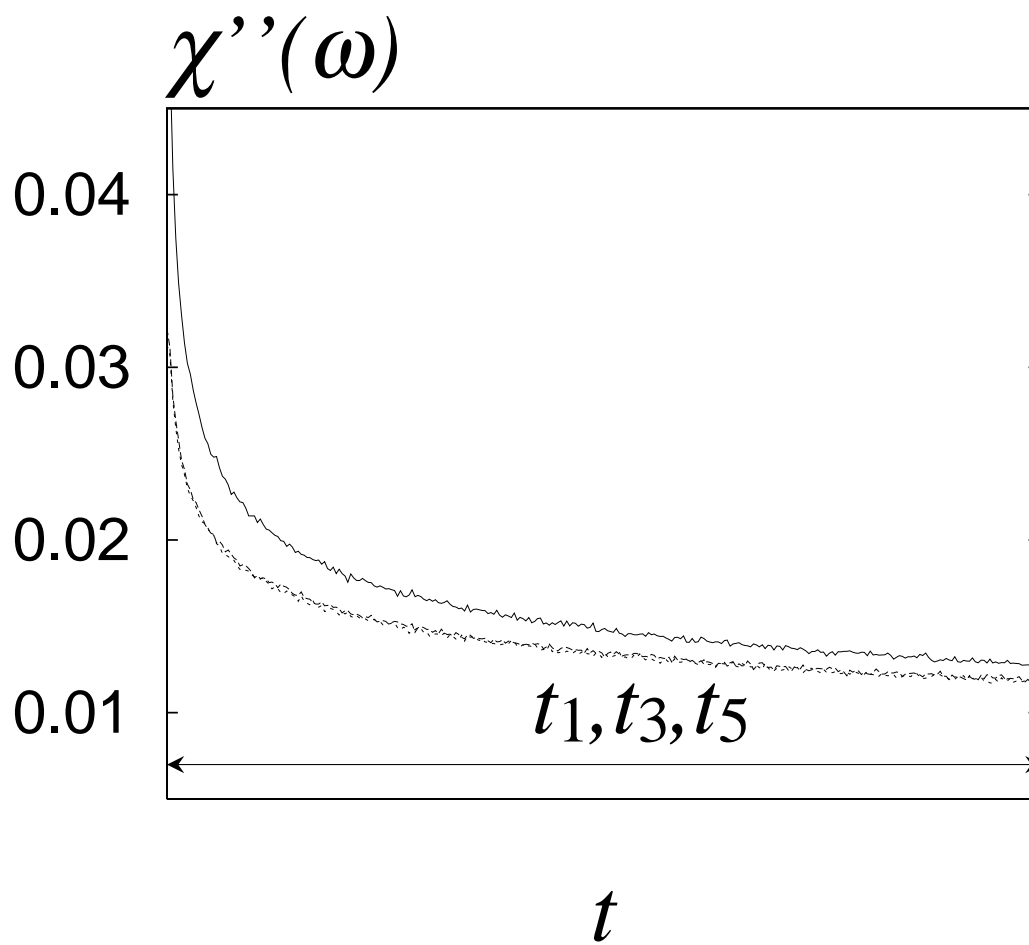


Fig.12

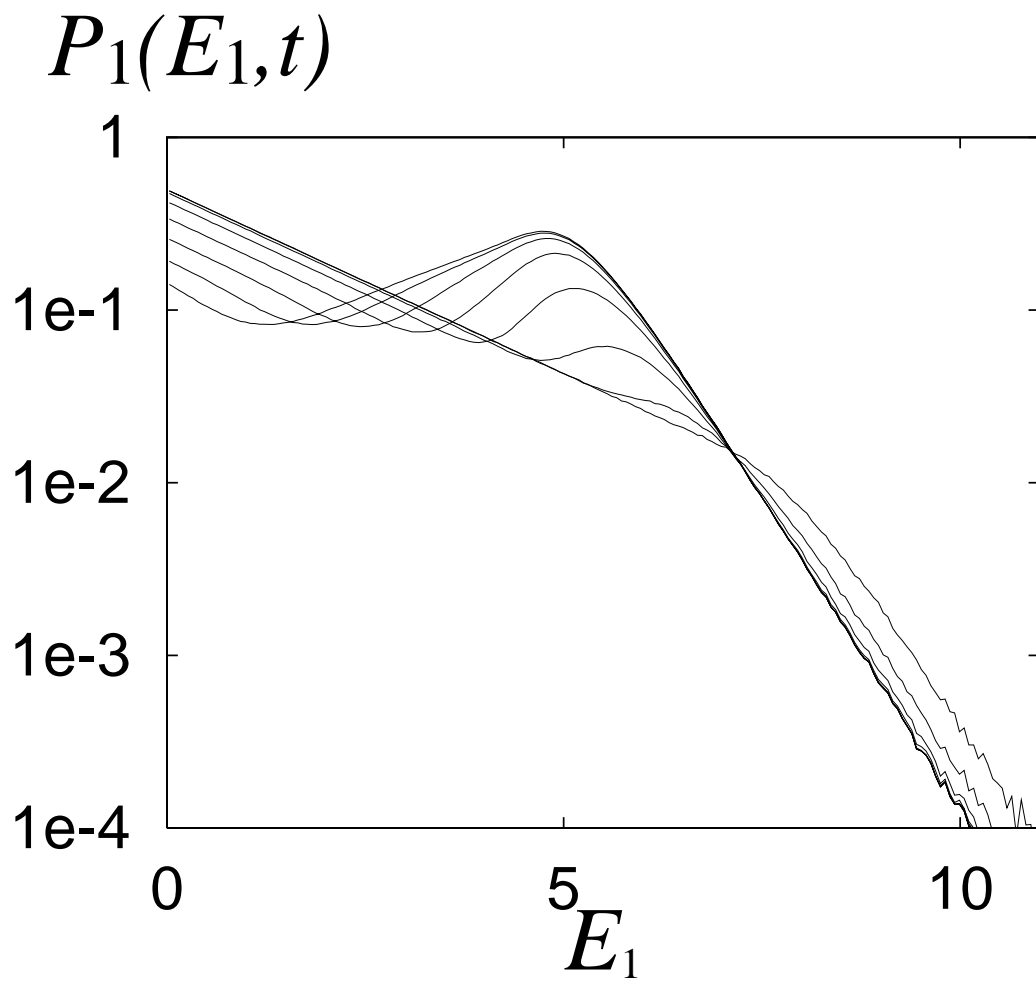


Fig.13